Hele-Shaw scaling properties of low-contrast Saffman-Taylor flows

M. W. DiFrancesco and J. V. Maher
Department of Physics and Astronomy, University of Pittsburgh, Pittsburgh, Pennsylvania 15260
(Received 20 December 1988)

We have measured variations of Saffman-Taylor flows by changing dimensionless surface tension B alone and by changing B in conjunction with changes in dimensionless viscosity contrast A. Our low-aspect-ratio cell permits close study of the linear- and early nonlinear-flow regimes. Our critical binary-liquid sample allows study of very low values of A. The predictions of linear stability analysis work well for predicting which length scales are important, but discrepancies are observed for growth rates. We observe an empirical scaling law for growth of the Fourier modes of the patterns in the linear regime. The observed front propagation velocity for side-wall disturbances is constantly 2 ± 1 in dimensionless units, a value consistent with the predictions of Langer and of van Saarloos. Patterns in both the linear and nonlinear regimes collapse impressively under the scaling suggested by the Hele-Shaw equations. Violations of scaling due to wetting phenomena are not evident here, presumably because the wetting properties of the two phases of the critical binary liquid are so similar; thus direct comparison with large-scale Hele-Shaw simulations should be meaningful.

I. INTRODUCTION

In this paper we report the results of systematically varying the control parameters for Saffman-Taylor[1] flow at low viscosity contrast. The cell we have used has a small aspect ratio [(length)/(width)=1] to allow us to study the linear regime and the earlier stages of nonlinear pattern formation. Most previous work[1-4] on this instability has used a high aspect ratio to reach and study the steady state, and indeed the detailed understanding of the steady state and its dependence on cell properties represents a noteworthy recent success of condensed-matter physics, and a fascinating example of the interdependence of theory and experiment.[1,2,4-7] Most previous experiments have also involved a high viscosity contrast between the two fluids in the flow.[1-4,8] There is general agreement that the same steady state should eventually be reached for both high- and low-contrast flows,[1,6] but the dynamical equations of the flows are explicitly contrast dependent, affecting at least the time scale over which the steady state is reached and possibly affecting the pattern evolution in much less trivial ways. In reports on earlier phases of our work[9,10] we have shown that the low-contrast flows in fact evolve not just more slowly than their high-contrast analogs, but also exhibit different morphology changes as they evolve.

The two control parameters[11] for the Saffman-Taylor flow are the dimensionless viscosity contrast A and the dimensionless surface tension B, both defined in Sec. II. We have varied B independently and also varied A and B in a locked way. We find good agreement in many of the measures of the flow with the scaling suggested by the Hele-Shaw equations. This is slightly surprising since work at high contrast, both in rectangular[2] and in circular[12] Hele-Shaw cells, shows significant breakdowns in the scaling; these breakdowns have been well explained in terms of wetting effects[5] which destroy the pure two-dimensional nature of the flow. While the discussion below will show that we do not fully understand the reason that wetting effects seem so negligible for the present case, it is hoped that the fact that the Hele-Shaw scaling is observed to apply to this case will encourage more extensive computer simulations of the A-dependent time evolution of this simplest of all pattern formation problems. In particular, fascinating simulations of the evolution of various solidification patterns have resulted from adding experimental or numerical anisotropies to the basic Hele-Shaw situation;[13] a serious quantitative test for the numerical simulations would be to reproduce in detail the results of the present simpler experiment.

Since in the linear regime the Saffman-Taylor instability is known to be broadband;[14] it is important to know which of the various possible flow measures exhibit large fluctuations and how rapidly these fluctuations are reduced as the steady state is approached. It is obvious that an empirical determination of the size of such fluctuations is very tedious, and in a case where fluctuations dominated the flow, computer simulations, provided one were sure that they incorporated all the "right" physics, would have a significant advantage over laboratory experiments. We have recently completed a study[10] of fluctuations in this system, wherein we measured a small "ensemble" of 14 realizations of the flow for essentially identical values of A and B. While the observed fluctuations are significant, they are not so large as to obscure the systematics to be presented below. In this paper we will assign uncertainties to each of our measurements on the assumption that they are the same as those measured in our ensemble.

In Sec. II we present details of the experiment, and define the control parameters and the important observables. In Sec. III, the results of our measurements are presented, and Sec. IV contains a discussion of the significance of our results.

II. EXPERIMENT

Reference 10 contains a description of the details of our apparatus and data reduction methods. Here we will only sketch the important features of the experiment, with particular emphasis on those features most crucial to the present measurements. The Saffman-Taylor instability arises at the initially planar interface between two fluids flowing in a Hele-Shaw cell (a cell formed by parallel plates with a gap between them of thickness b, which is smaller than any other length scale in the problem). The instability is driven either by a pressure gradient advancing the less viscous fluid against the other or by gravity as a result of a density difference between the fluids. In the present case, we use a closed cell (thus the average velocity of the interface is constrained to be zero) and drive the instability gravitationally; we initiate the flow by rotating the cell to raise the more dense fluid above the less dense. In this case, the dispersion relation from linear stability analysis[14] takes the form

$$i\omega(2\bar{\mu}/K)-(\rho_2-\rho_1)gk+\sigma k^3=0 , \tag{1}$$

where $K=b^2/12$ is a mobility. The average shear viscosity, the interfacial surface tension, the density of fluid n, and the acceleration due to gravity are $\bar{\mu}$, σ, ρ_n, and g, respectively. This dispersion relation predicts broadband instability for all wavelengths λ above a critical value

$$\lambda_c=2\pi[\sigma/(\rho_2-\rho_1)g]^{1/2} . \tag{2}$$

The fastest growing mode $\lambda_{\max}$ is expected to be that with wavelength $\sqrt{3}\lambda_c$. Tryggvason and Aref[11] (TA) have shown that the problem can be cast in terms of two control parameters A and B, where A is the dimensionless viscosity contrast

$$A=\frac{\mu_2-\mu_1}{\mu_2+\mu_1} , \tag{3}$$

and B is the dimensionless surface tension (or inverse capillary number)

$$B=\sigma b^2/[6U^*W^2(\mu_2+\mu_1)] , \tag{4}$$

with W the width of the Hele-Shaw cell and U^* the characteristic velocity

$$U^*=\frac{(\rho_1-\rho_2)gb^2}{12(\mu_1+\mu_2)} . \tag{5}$$

TA shows that B can be scaled out of the two-dimensional Hele-Shaw equations by adopting the dimensionless time

$$t'=U^*t/1.84WB^{1/2} , \tag{6}$$

and the dimensionless length

$$x'=x/7.70WB^{1/2} . \tag{7}$$

We have added the factors 1.84 and 7.70 in Eqs. (6) and (7) to make the fastest-growing wavelength $\lambda_{\max}=1$ and the growth rate of $\lambda_{\max}$ (from the linear stability analysis) also equal 1. As was mentioned above, the viscosity contrast A cannot be scaled out of the equations.

In this experiment we exploit the well-known features of critical binary liquids to vary the control parameters of the Saffman-Taylor flow. This not only eliminates the need to change liquids when varying the control parameters, but it also provides great precision in the knowledge of and changes in the control parameters. For a critical binary liquid[15] in the two-phase region, the density difference depends on reduced temperature $\epsilon=(T_c-T)/T_c$, where T_c is the critical temperature, as $\Delta\rho=\rho_0\epsilon^{\beta}$, where $\beta=\frac{1}{3}$ and interfacial tension, $\sigma=\sigma_0\epsilon^{\mu}$, where $\mu=1.25$. Since kinematic viscosity is, to a very good approximation, the same for both phases, the difference in shear viscosities between the two phases has the same temperature dependence as does the mass-density difference. Using the measured critical coefficients for the isobutyric acid–water system[16] used in this experiment, one finds the fastest growing wavelength and the control parameters as follows:

$$\lambda_{\max}=\lambda_0\epsilon^{0.45} , \tag{8}$$

$$A=0.027\epsilon^{1/3} , \tag{9}$$

$$B=0.022\epsilon^{0.92}(\cos\alpha)^{-1} . \tag{10}$$

During the course of this experiment we varied the control parameters in two ways. In method 1, B could be varied while A was held constant by varying the angle α between the plane of the cell, and the vertical to control the effective gravitational acceleration g. In method 2, by changing temperature, A and B could be changed together according to relations (9) and (10) above.

As was mentioned above, wetting effects are known to modify the Hele-Shaw equations, and the destruction of Hele-Shaw scaling by such effects has been observed in both rectangular[2] and radial[12] Hele-Shaw cells for air-oil interfaces. Thus the scaling results to be presented below are anything but a forgone conclusion. Our cell gap $b=1$ mm is smaller than, but not much smaller than, the 4.5–8-mm wavelengths observed in the patterns to be discussed below. Other than for wetting corrections to the two-dimensional equations,[2] it is difficult to estimate the length-scale ratio at which three-dimensional effects should become important, but a previous study[9] suggests that a 4.5:1 ratio produces results which are similar to flows at much larger ratio and that observable three-dimensional effects set in very gently near a ratio of 3:1. We conclude this section with a list of the experimental peculiarities of the present work which (i) are different from some or all of the previous work on this instability and/or (ii) could conceivably require modification of the Hele-Shaw equations. First, the wetting properties of the liquids: in most previous experiments the invading fluid either preferentially wets the walls or it leaves behind an intact wetting layer of the displaced fluid, the latter being the case for air-oil interfaces. In the present case the two phases of the binary liquid are very similar in their wetting properties, and, at equilibrium a few hundred millikelvins below the critical temperature, the water-rich phase is slightly preferred by the glass (contact angle $\approx 70°$). Second, flexing of the glass plates of the cell is much less a problem in the present case than in most other experiments, both because the cell is surrounded by the water of the temperature control bath, which is at essen-

tially the same pressure as the inside of the cell, and because the pressure differences built up between the nearly identical phases inside the cell are so small. Finally, the cell is closed and gravity driven, with no externally applied pressure gradient and no liquid of either phase entering or exiting. The possible influence of these experimental differences will be discussed in Sec. IV below.

III. RESULTS

We will arbitrarily divide our presentation of results and their subsequent discussion into those with implications mainly in the linear regime and those which still apply after the system has passed over into the nonlinear regime. As was discussed in some detail in Ref. 10, we find that many flow properties change markedly between these regimes if we define the regime boundary to come at the time when the amplitudes of the central fingers (i.e., excluding the last finger on each side of the cell) become equal to the mean wavelength of the pattern.

A. Linear regime

Figure 1 shows mean wavelength (defined as cell width $W=4.5$ cm divided by the number of fingers) as a function of reduced temperature. The uncertainties shown in the figure are standard deviations resulting from repeating each measurement about 15 times under as close to identical conditions as the apparatus allows. Each measurement provides a well-defined integer for the number of fingers appearing in that realization, and the error bars represent a measure of the reproducibility of this aspect of the flow. It is interesting to note that the standard deviations are quite uniform whether or not the mean number of fingers is close to an integer value. One might expect the pattern to lock in slightly better when the cell width and capillary length become commensurate, but if this is correct, the matching requirement is too severe for us to accidentally meet it. (There is one point in the figure where all 15 flows gave the same number of fingers, but with the typical observed standard deviations, the fluctuations expected for samples of size 15 should give about this many such points.) The ensemble whose analysis has provided the estimates of uncertainties used in this paper appears as the point at $\epsilon=6.12\times10^{-3}$ in Fig. 1.

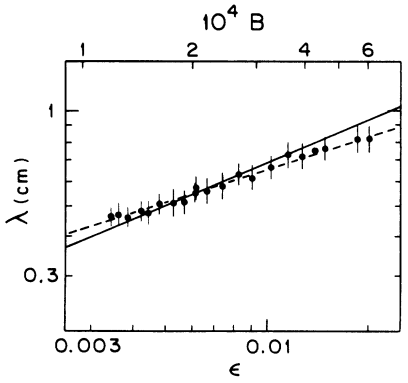

FIG. 1. Mean finger wavelength λ vs ϵ, the reduced temperature. Also shown on the upper edge is dimensionless surface tension B calculated from ϵ using Eq. (10). Over this same range of data, the dimensionless viscosity contrast A, calculated using Eq. (9), varies from 4.06×10^{-3} to 7.37×10^{-3}.

The solid curve in Fig. 1 results from a best fit to the data using the power law of Eq. (8) with the expected combination of known critical exponents. If we allow the exponent to vary, the best power-law fit to the data produces the dashed curve in the figure and yields an exponent 0.34 ± 0.08. We do not regard as significant the approximately one standard deviation difference between the best-fit exponent and the expected value because the observed range of reduced temperature is only about a decade. The coefficient λ_0 from Eq. (8) is 5.4 if one uses the exponent 0.45 and 3.1 if one uses exponent 0.34. The available values of the critical coefficients which combine to produce λ_{max} predict a value of $5.1\pm12\%$. Again the agreement is sufficient to suggest that the linear stability analysis is rather accurate. Most authors[8,14] of previous works have reported only qualitative results for their $A\sim1$ work in the linear regime, but Park *et al.*[3] report for $A\sim1$ an agreement between observed λ and the linear theory expectation which is quite similar to the present $A\sim0$ result.

In Ref. 10 we reported that we could observe the linear pattern setting up, activated by an initial disturbance at the sidewalls which propagates across the relatively flat interior of the interface. One presumes that the same linear pattern would eventually be set up if there were no side walls (and we have, indeed, qualitatively verified this by observing the same flows in an annular Hele-Shaw cell), but it would almost certainly take a much longer time to get started. All other reported rectangular Hele-Shaw flows see side-wall disturbances,[2–4,8] and indeed the side-wall influence dominates the eventual steady state, but here we have slowed the instability sufficiently (and correspondingly reduced the side-wall disturbance by using liquids of such closely matched properties) that we can study the progress of the side-wall disturbance into the interior of the cell. Figure 2 shows the position of the propagating front as a function of time as the side-wall disturbance moves toward the center of the cell. In the upper part of the figure, the data for several values of control parameter B (with A fixed at 6.9×10^{-3}) are shown in dimensional form. In the lower part, the data have been scaled to dimensionless form by using Eqs. (6) and (7). The earliest-time data show a dimensionless propagation velocity $V^*=0.8$, while the later-time data suggest $V^*=3.7$. If we make the admittedly crude approximation that the linear pattern, which is slowly forming, is a steady state toward which the propagating disturbance is driving the system, then the formalisms of Langer[17] and van Saarloos[18] can be applied. Both formulations of our problem[19] predict $V^*=\sqrt{3}$ in our dimensionless units.

Additional insight into pattern development in the linear regime can be gained by considering the Fourier transforms of the patterns. Following the results we reported in Ref. 10, here and below for our discussion of

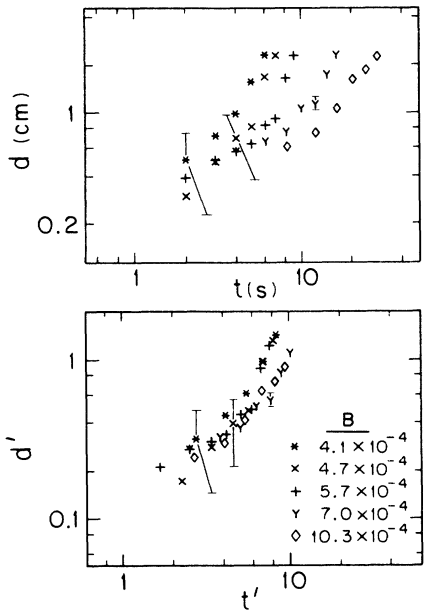

FIG. 2. Top: Propagation distance of the initial side-wall disturbance d vs time. Bottom: The same plot in dimensionless units.

the nonlinear regime we will turn the patterns into single-valued functions by considering x, position across the cell, and y, position in the flow direction, as functions of total arc length s. Figure 3 shows a temporal sequence of "power spectra" from the Fourier transform of y versus arc length. The parabolic curve in the figure is the

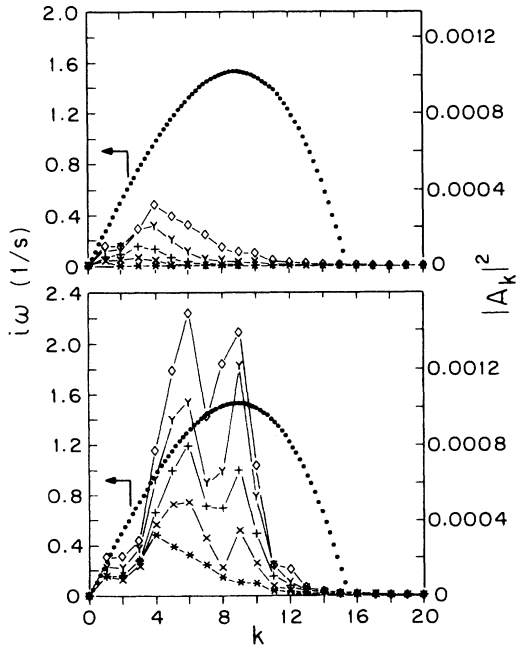

FIG. 3. Top: The dotted line shows the growth rate $i\omega$ as a function of wave number k as given by the linear stability dispersion relation. All other symbols show the progression, for the first 5 sec, of the power spectrum $|A_k|^2$ vs k. Bottom: The same plot for 5–9 sec. Wave numbers are in fractions of inverse total arc length. $|A_k|$ is in units of the cell width.

growth rate as a function of the wave number from the linear stability analysis. The data are not exactly comparable to the linear stability dispersion relation because the wave numbers for the dispersion relation are in units of inverse cell width $1/W$, while the successive power spectra have changing wave-number units, each being in units of its own inverse integrated arc length. Nevertheless, in the linear regime the arc length is not much longer than the width of the cell ($\leq 2W$) and the growth of the power spectra seem to follow the prediction of the dispersion relation rather well. Figure 4 shows more detail on the temporal development for several wave numbers from the same flow realization analyzed in Fig. 3. Here we encounter a puzzling result. If we look just at the Fourier amplitudes, the "right" wave numbers dominate the flow with higher and lower wave numbers much less important (see the linear scale in the top half of Fig. 4.) However, if we examine the log of the Fourier amplitudes (lower half of Fig. 4), essentially all wave numbers show the same growth rate in the linear regime (for this flow, the pattern passed out of the linear regime at about $t=6$ in dimensionless units); this growth rate is 0.45 in dimensionless units, where the linear stability analysis predicts 1.

Park *et al.*[3] report a similar result for their $A\sim 1$ work; however, they observe constant growth rate for all wave numbers only for capillary numbers $N_{\rm cap} < 5\times 10^{-3}$, where

$$N_{\rm cap} = \frac{1}{12}\left(\frac{b}{W}\right)^2 \frac{1}{B} . \tag{11}$$

In terms of B, our $A\sim 0$ data almost completely overlap their range of B ($1.5\times 10^{-4} \leq B \leq 1.0\times 10^{-3}$ for the

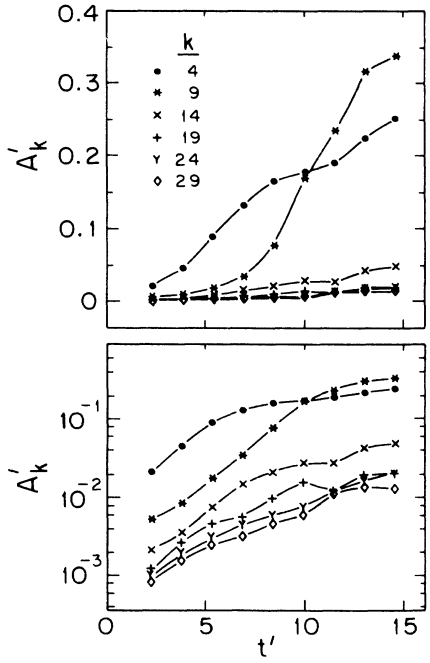

FIG. 4. The dimensionless Fourier amplitude A'_k vs dimensionless time for the wave numbers indicated.

present work as opposed to $1.2\times10^{-4}\le B\le9\times10^{-4}$ for Park *et al.*[3]). In terms of N_{cap}, our data sample much larger capillary numbers than those of Park *et al.* ($0.04\le N_{cap}\le0.27$ versus $1.5\times10^{-3}\le N_{cap}\le8.5\times10^{-3}$, respectively). In either case we observe the constant-growth-rate effect in a range not seen near $A=1$. Park *et al.* attributed this effect to the nearness of side walls, arguing that at low capillary number, their number of fingers was small and their growth rates were too small relative to the advance of the interface. In the present case their arguments do not seem relevant because (i) our capillary numbers and numbers of fingers are much larger, and (ii) the average velocity of our interface is zero, so sidewall pinning should not involve having the advancing interface leave the sides behind at a rate large in comparison with the pattern growth rate. The two effects in Fig. 4 present an interesting puzzle. The close correspondence between the Fourier amplitudes and the expected shape of the dispersion relation suggests that the linear stability theory has worked rather well at some early time, but the constant growth rates for all wave numbers indicate that it no longer works well at times when the pattern amplitudes A_k are still much less than the dominant wavelengths $1/k$ ($A_k k\sim10^{-2}$). We do not understand this effect. We find an empirical scaling rule for the power spectra in the linear regime. The relation

$$P(k)=|A_k|^2=Ct^p f(akt^{-q}) , \tag{12}$$

where C and a are nonuniversal constants and f, a scaling function, can collapse the power spectra if we use the parameter values $p=2.5$ and $q=0.5$. This is illustrated in Fig. 5, where the unscaled power spectra are shown in the upper part and the scaled results ($|A_k|^{2\prime}=|A_k|^2t^{-p}$ versus $k'=kt^{-q}$) appear in the lower part. We know of no theoretical justification for this result, but hope that its empirical observation will prove fruitful.

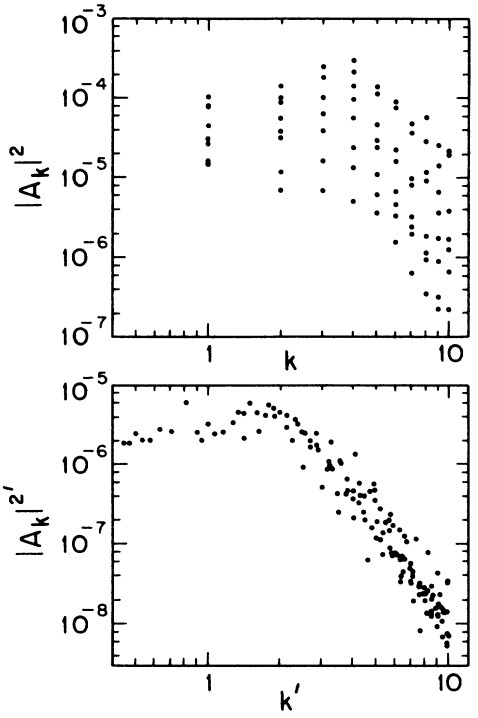

FIG. 5. Top: Power spectra at several times in the linear regime superimposed. Wave numbers are in fractions of total arc length. $|A_k|$ is in units of the cell width. Bottom: Scaled power $|A_k|^{2\prime}=|A_k|^2t^{-p}$ vs scaled wave number $k'=kt^{-q}$.

B. Parameter variations and scaling in the linear and nonlinear regimes

In this section we consider several measures of the flow and examine the collapse of the data when realizations representing a variety of control parameter values are presented in dimensionless form. As was mentioned above, we assume that the fluctuations in Ref. 10 are typical of those which would be encountered if each control point presented here were measured many times, and the averages and standard deviations constructed. Accordingly, we place several representative "error bars" on each figure to show the reader the size fluctuations which might be expected and to allow the reader to assess the quality of the collapse of the dimensionless data. These "error bars" are frequently drawn slanted out of the vertical to avoid obscuring other data points; they refer in all cases to uncertainty in the ordinate alone.

Figure 6 shows the length of the mixing zone Θ versus time. Time is presented in seconds in the upper part of the figure and in dimensionless units below. As is indicated in the figure, these data were measured with a constant contrast $A=6.9\times10^{-3}$, and have a wide variety of values of the control parameter B (achieved by method 1,

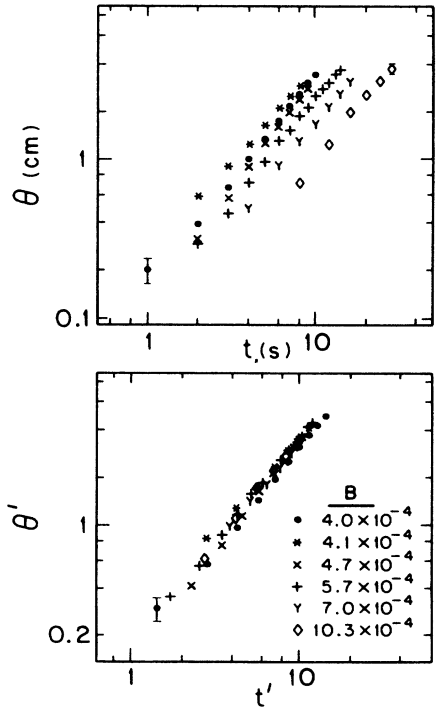

FIG. 6. Top: Width of finger pattern in the direction of growth Θ vs time for flows with differing values of B, the dimensionless surface tension. B was varied using method 1. Bottom: Θ', the dimensionless finger pattern width, vs t', the dimensionless time.

varying the tilt angle of the cell). The collapse is impressive. In Fig. 7 the collapse is less impressive; the data in this figure, obtained by method 2, differ in the temperature value at which the cell was held, and thus involve variations of both A and B. The less impressive collapse does not necessarily indicate any failure of the scaling; rather the unscaled data in Fig. 7 do not differ much in the first place, despite the fact that the wavelength (number of fingers) changes by a factor of 1.7 over the range of these data. Maxworthy[8] also observes a collapse of Θ' versus t' when he varies B for his $A \sim 1$ system. Since the dimensionless Hele-Shaw equations themselves retain an A dependence, it is instructive to ask how great an A dependence appears in the data. It is clear that the data of Fig. 7 retain little A dependence, as A varies by a factor of 1.4. In Fig. 8 we compare the data of Fig. 6 with large-A data borrowed from Ref. 9; over this large difference in A a substantial difference in the data survives the scaling. Following TA, we define a dimensionless interfacial stretching

$$L'(t)=\frac{L(t)}{L_0}-1 \ , \tag{13}$$

where L_0 is the length of the initial interface (identical to cell width W in all cases presented here), and $L(t)$ is the length of the interface at time t. Figure 9 shows the quality of the collapse of $L'(t)$ for data with constant A and various values of B when the time is made dimensionless. When temperature is used to vary both A and B, the variation in the unscaled data is again less dramatic, but

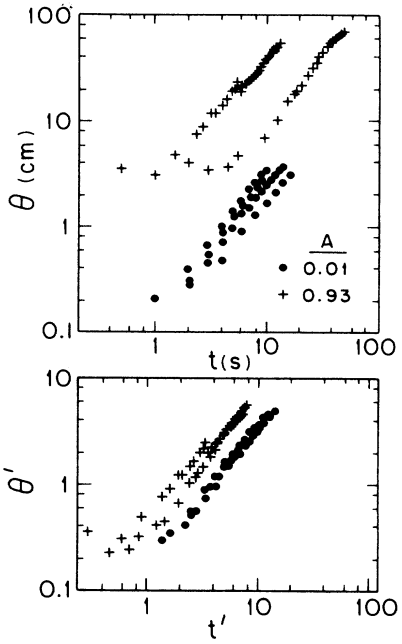

FIG. 8. Comparing Θ vs t for a group of flows at $A \sim 1$ and a group at $A \sim 0$. Bottom: Comparison after scaling to dimensionless units.

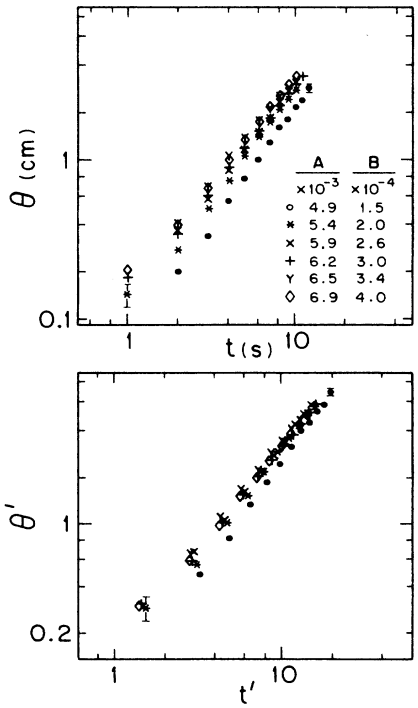

FIG. 7. Θ vs t for flows with different values of both A and B. Flow parameters were varied using method 2. Below is the scaled version.

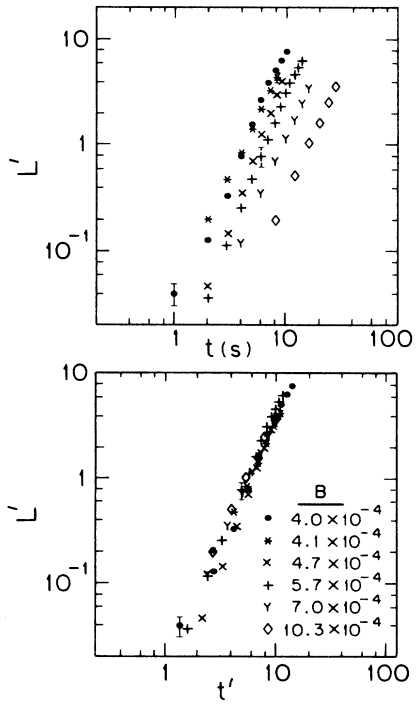

FIG. 9. Dimensionless stretching L' vs time in seconds for flows differing in B only. Below is shown L' vs t', dimensionless time.

the collapsed data overlap just as well. Maxworthy's L' versus t' data[8] for $A \sim 1$ do not collapse under this scaling. The average magnitude of the curvature of the two-dimensional pattern was found in Ref. 10 to have a maximum value just at the time that the patterns passed out of the linear regime. This quantity is shown for both methods of control parameter variation in Figs. 10 and 11, again in both dimensional and dimensionless form. As was the case for the other quantities, the collapse is impressive. We can see that under a wide variety of conditions the system tends to reach this curvature maximum and enters the nonlinear regime at roughly six units of dimensionless time. We have also performed a modal analysis of the present data, avoiding the problem that the patterns are not, in general, single-valued functions of distance across the cell by resorting to separate analyses of the functions $x(s)$ and $y(s)$ discussed briefly above and in great detail in Ref. 10. The amplitude of any individual Fourier mode in this analysis is quite uncertain because the instability is broadband; in Ref. 10 we found that even the most important individual modes were subject to 50% fluctuations. However, we always do observe the same general behavior reported in Ref. 10; viz, the power spectra for both $x(s)$ and $y(s)$ are both dominated by low wave numbers (especially $k=1$) at early times, and then a second maximum in the power spectrum grows at later times and at larger wave numbers. The low-wave-number maximum is closely associated with the side-wall interaction, while the second maximum corresponds closely to what one might expect from the linear stability theory. We have summed the strengths of the squared Fourier amplitudes for each of these four

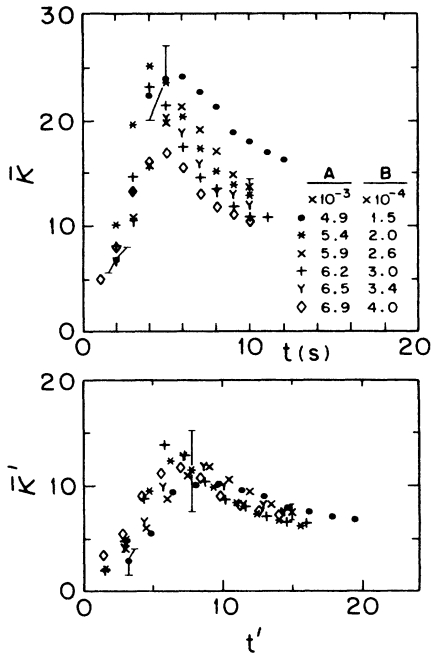

FIG. 11. Average curvature vs time for flows differing in A and B. The unscaled data (top plot) are compared to the scaled data (bottom plot).

maxima as a function of time, and these are shown in Figs. 12–15. (In these figures,

$$\sum_{i,j} = |A_{j-1}|^2 + |A_j|^2 + |A_{j+1}|^2 , \tag{14}$$

where A_j, is the Fourier amplitude for the mode $k=j$ and the function $i=x$ or $i=y$.) In Fig. 12, the low-

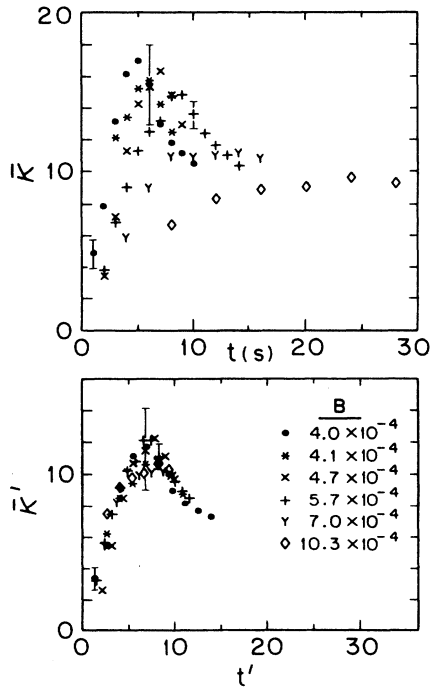

FIG. 10. Average curvature $\bar{\kappa}$ vs time for flows at different B. The bottom plot shows the same data in dimensionless units.

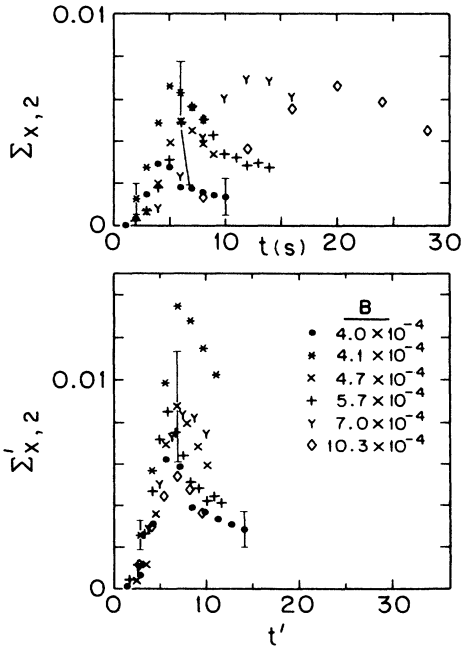

FIG. 12. Power in the first three Fourier modes of $x(s)$ vs time shown unscaled (top) and scaled (bottom).

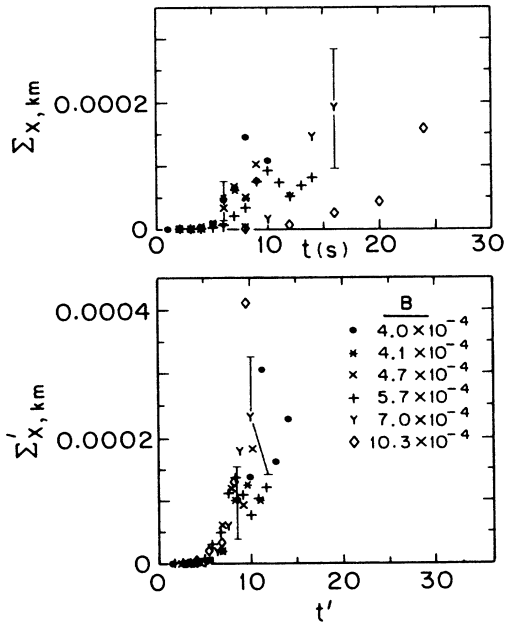

FIG. 13. Power in the three Fourier modes of $x(s)$ centered around the fastest growing mode as given by the linear dispersion relation vs time. On top are the unscaled data and below the data are shown scaled.

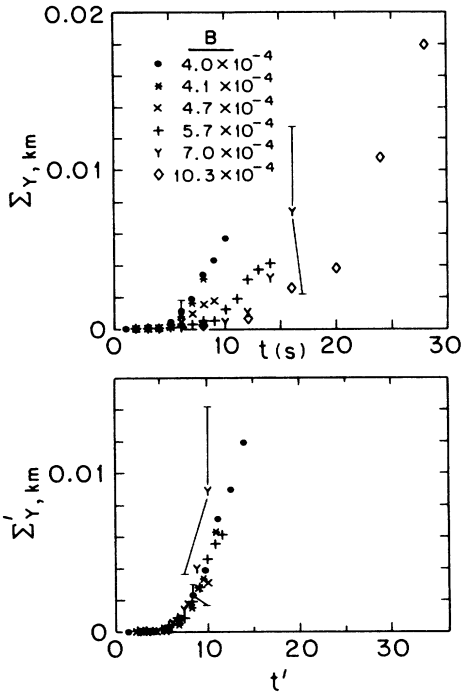

FIG. 15. Power in the three Fourier modes of $y(s)$ centered around the fastest growing mode as given by the linear dispersion relation vs time. On top are the unscaled data and below the data are shown scaled.

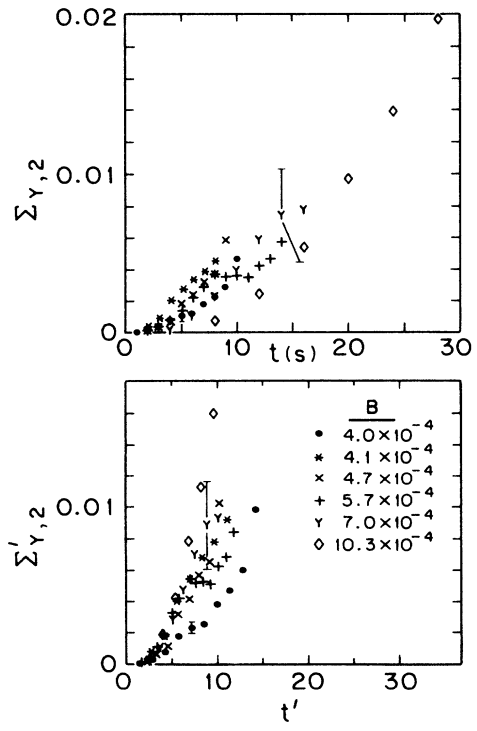

FIG. 14. Power in the first three Fourier modes of $y(s)$ vs time shown unscaled (top) and scaled (bottom).

wave-number sum for $x(s)$ shows a maximum which is normally reached at six units of dimensionless time. We do not understand the failure of the magnitude of the sum to collapse for the case $B=4.1\times10^{-4}$, but otherwise the sums, in dimensionless units, reduce to roughly the same form within the limits of the expected fluctuations. Figure 13 shows the sum for the region of the second maximum in the $x(s)$ power spectrum. Here the data collapse nicely for dimensionless times below 7, but become quite noisy as the nonlinear regime is entered. The situation is similar for both maxima in the typical $y(s)$ power spectrum, Figs. 14 and 15. The sums collapse rather well at early times but diverge well outside expected fluctuations at later times.

IV. DISCUSSION

While several of the results presented above have self-evident implications for our understanding of this pattern evolution problem, several others require further discussion. As before, we divide our discussion according to the two general questions addressed in this paper: (i) How well do we understand the linear regime, and (ii) how well can the pattern evolution be scaled in dimensionless form? In Sec. III it was clear that λ_{max}, the fastest growing wavelength, is quite well predicted by the standard linear stability analysis. Similarly, the entire dispersion relation from the linear stability analysis is at least qualitatively reproduced by the power spectra of $y(s)$. On the other hand, the measured growth rates of

the various wave numbers all appear about the same in Fig. 4, at least until the patterns are well into the nonlinear regime; this makes no sense in terms of the standard theory. The empirical scaling of the power spectra is intriguing and, as far as we know, unexpected. Jasnow has reported a similar scaling for a computer simulation of the growth of unstable magnetic domain walls.[20] Our exponents are very different from Jasnow's but his problem is somewhat different and, in addition, our order parameter is conserved while his is not. It is interesting to note that, by watching the initial disturbance propagate from the noisy (side-wall) part of the interface to the quiet (central) part, we can observe a characteristic propagation rate which scales roughly with the Hele-Shaw velocity scale. This is in agreement with the results of Langer[17] and van Saarloos[18] who predicted that the transverse front velocity should come directly from the linear dispersion relation. Both formulations give a prediction of $\sqrt{3}$. We observe a slightly lower velocity at first (0.8), with a growth to 3.7 shortly before the fronts from opposite sides of the cell join each other at the center. It is difficult to assess the importance of the discrepancy (nonconstancy of our velocity) since van Saarloos's and Langer's formulations are meant to apply to a front which is setting up a steady state; our comparison is valid only insofar as the linear pattern which is being set up can be regarded as a substitute for a steady state toward which the system is at least temporarily evolving. Applying the theory to our case is less trustworthy at both the earliest times (when there is a wall rather than an established pattern immediately behind the front) and at the latest times (when the two fronts are near and presumably attract each other). Thus the most reasonable way to state our result is to say that we see $V^*=2\pm1$. Turning our attention now to the second issue of scaling effects in the pattern evolution, it is clear that there is a very impressive collapse of most of the data in Figs. 6–15 when they are presented in dimensionless form. This is especially impressive for the results (Figs. 12–15) for the evolution of the power spectra of the functions $y(s)$ and $x(s)$. These functions contain within them all the rich detail of the original highly ramified patterns $y(x)$, and thus correspond to a wide variety of numbers of fingers (ranging from 5 to 10), and of development of ballooning finger tips (see Ref. 10 for a discussion of the morphology of patterns). Yet despite the great variety of pattern detail, the power spectra have their dominant features apparently universal, with the only nonuniversal feature being the need to shift the power sums shown in Figs. 13 and 15 to be over the observed second maxima, which vary in maximum-strength wave number in just the way one would expect from the linear stability analysis. The success of the Hele-Shaw scaling not only includes a reasonably large range of the inverse capillary number B, but also includes data which attain similar values of B in different ways (with and without changes in surface tension, and thus in wetting properties). This success, not seen in the available large-A experiments,[2,5] including our own,[12] is an indication that the Hele-Shaw equations are a reasonably good approximation to the physics which determines the behavior of this system. This result suggests that it is worthwhile to undertake extensive computer simulations for this case to see how well calculations can reproduce such an unusually simple pattern growth problem. Even as we suggest that this case may be an unusually simple one, well suited to simulation with a two-dimensional approximation, we must discuss a significant misgiving; we do not understand why this case is different from the high-contrast cases. In trying to understand why this case seems different, we can raise several issues.

(i) The wetting properties are different. The two phases of the critical binary liquid wet the wall almost equally well, and this may make the difference. On the other hand, if one makes the naive assumption that the wetting correction of Park and Homsy[5] (suited to the very different case where the displaced liquid wets the wall, leaving behind a thin film whose thickness depends on the local interfacial velocity) provides a reasonable first-order estimate of our wetting-curvature correction, then the known power laws for interfacial tension and density contrast near the critical point actually make the wetting correction diverge as the critical point is approached. That is, interfacial tension vanishes as $\epsilon^{1.25}$ so that the first correction term in the expansion of Park and Homsy would vary as $\epsilon^{-0.61}$. Of course, in our case the displaced fluid should leave behind a thin film whose curvature depends at least partly on local velocity because of contact-angle hysteresis, but the functional dependence for incomplete wetting should not, in general, be the same. Furthermore, our interface is divided roughly equally between regions where the better-wetting liquid is being displaced and regions wherein this liquid is intruding. We have not succeeded in constructing a convincing argument to handle this case, but the empirical results presented above do suggest that the wetting effects are much less important here. (ii) The present case involves a closed cell. This was discussed in Sec. II, but in the present discussion, it is well to remember that closing the cell imposes a mass-conservation law on each phase of the liquid, a situation which may differ from that of pressure-driven flow between reservoirs in ways not unlike the differences between critical systems with conserved and nonconserved order parameters. It is also worth reemphasizing that the small size of the cell is not a very important feature of the present system. In Ref. 10 we reported that no qualitative changes occurred in the stages of the flow presented above when the length of the closed cell was increased by a factor of 5. (iii) The roles of gravity and the pressure gradient are very different in the present case than in most previously studied systems. These two sources of driving force for the instability are known to be completely equivalent once the steady state is set up and also appear equivalent in the linear stability analysis, but for different reasons. It has been pointed out to us[21] that the two sources have different effects on the Gibbs-Thompson relation for the pressure jump at the interface during the intermediate stages of the flow, and thus may involve a nontrivial difference for a case like ours. In most of the literature this is assumed not to be the case, and it would be most intriguing to find, through simulation, that there was

indeed a significantly different role for gravity than for a pressure gradient in this case. Unfortunately, we cannot at present comment on this possibility in much more detail. We can, however, point out that, at high A, Maxworthy[8] has reported results in a closed gravity-driven cell that are very similar to those which we and others have reported for an open pressure-driven cell. We have also qualitatively verified Maxworthy's results in our own closed high-A cell (air-oil).

V. SUMMARY AND CONCLUSIONS

We have measured variations in Saffman-Taylor flows by changing dimensionless surface tension B alone and by changing B in conjunction with changes in dimensionless viscosity contrast A. Our low-aspect-ratio (i.e., wide) cell permits close study of the linear and early nonlinear regimes. We find that the predictions of linear stability analysis work well for all predictions for which length scales are important, but that there is an observed discrepancy in growth rates. This is reminiscent of some of the results found by Chou and Cummins[22] and by Dougherty *et al.*[23] for the linear regime in the related cases of directional solidification and dendritic growth in supersaturated solutions. We observe an empirical scaling law for the growth of the Fourier modes in the linear regime. The observed front propagation velocity (as the initial disturbance works its way out from the side walls along the initially flat interface, setting up the expected linear-regime pattern) is consistently 2 ± 1 in dimensionless units, a value which overlaps the predictions of Langer[17] and van Saarloos.[18] Data in the nonlinear regime collapse impressively under scaling suggested by the Hele-Shaw equations (Figs. 6–11). Wave-number sums from a modal analysis constitute a partial exception: these collapse at early times but tend to diverge later (Figs. 12–15). We observe empirically that wetting causes much less dramatic departures from the Hele-Shaw scaling than in other systems for which this instability has been studied, presumably because the two phases of our critical binary liquid are so similar in their wetting properties. The success of Hele-Shaw scaling suggests that large-scale computer simulations of the Hele-Shaw equations for this simple case could provide a meaningful confrontation between experiment and theory.

ACKNOWLEDGMENTS

We deeply appreciate helpful discussions with W. I. Goldburg, D. Jasnow, J. S. Langer, S. Sarkar, and W. van Saarloos. This work has been supported by the U.S. Department of Energy under Grant No. DE-FG02-84ER45131.

[1]P. G. Saffman and G. I. Taylor, Proc. R. Soc. London, Ser. A **245**, 312 (1958); S. Hill, Chem. Eng. Sci. **1**, 247 (1952).

[2]P. Tabeling and A. Libchaber, Phys. Rev. A **33**, 794 (1986); P. Tabeling, G. Zocchi, and A. Libchaber, J. Fluid Mech. **177**, 67 (1987).

[3]C.-W. Park, S. Gorell, and G. M. Homsy, J. Fluid Mech. **141**, 257 (1984).

[4]G. M. Homsy, Ann. Rev. Fluid Mech. **8**, 233 (1987), and references therein.

[5]C. W. Park and G. M. Homsy, J. Fluid Mech. **139**, 291 (1984).

[6]D. Bensimon, L. P. Kadanoff, S. Liang, B. I. Shraiman, and C. Tang, Rev. Mod. Phys. **58**, 977 (1986).

[7]J. W. McLean and P. G. Saffman, J. Fluid Mech. **102**, 455 (1981); J. M. Vanden-Broeck, Phys. Fluids **26**, 2033 (1983); D. Kessler, J. Koplik, and H. Levine, Phys. Rev. A **30**, 3161 (1984); D. A. Kessler and H. Levine, *ibid.* **32**, 1930 (1985); **33**, 2634 (1986); D. Bensimon, *ibid.* **33**, 1302 (1986); S. Sarkar and D. Jasnow, *ibid.* **35**, 4900 (1987); A. T. Dorsey and O. Martin, *ibid.* **35**, 3989 (1987); B. I. Shraiman, Phys. Rev. Lett. **56**, 2028 (1986); D. C. Hong and J. S. Langer, *ibid.* **56**, 2032 (1986); R. Combescot, T. Dombre, V. Hakim, Y. Pomeau, and A. Pumir, *ibid.* **56**, 2036 (1986); A. J. DeGregoria and L. W. Schwartz, J. Fluid Mech. **164**, 383 (1986); S. Liang, Phys. Rev. A **33**, 2663 (1986); T. Vicsek, Phys. Rev. Lett. **53**, 2281 (1984); P. Meakin, F. Family, and T. Vicsek, J. Colloid Interface Sci. **117**, 394 (1987); J. Nittman, G. Daccord, and H. E. Stanley, Nature (Paris) **314**, 141 (1985).

[8]T. Maxworthy, J. Fluid Mech. **177**, 207 (1987).

[9]J. V. Maher, Phys. Rev. Lett. **54**, 1498 (1985); in, *The Physics of Finely Divided Matter*, edited by N. Boccara and M. Daoud (Springer-Verlag, Berlin, 1985), pp. 252–257.

[10]M. W. DiFrancesco and J. V. Maher, Phys. Rev. A (to be published).

[11]G. Tryggvason and H. Aref, J. Fluid Mech. **136**, 1 (1983); **154**, 287 (1986).

[12]S. N. Rauseo, P. D. Barnes, Jr., and J. V. Maher, Phys. Rev. A **35**, 1245 (1987).

[13]J.-D. Chen and D. Wilkinson, Phys. Rev. Lett. **55**, 1892 (1985); E. Ben Jacob, R. Godbey, N. D. Goldenfeld, J. Koplik, H. Levine, T. Mueller, and L. M. Sander, *ibid.* **55**, 1315 (1985).

[14]R. L. Chuoke, P. van Meurs, and C. Van der Poel, J. Pet. Technol. **11**, 64 (1959).

[15]H. E. Stanley, *Introduction to Phase Transitions and Critical Phenomena* (Oxford University Press, New York, 1971).

[16]S. C. Greer, Phys. Rev. A **14**, 1770 (1976).

[17]J. S. Langer in, *Chance and Matter*, edited by J. Souletie, J. Vannimenus, and R. Stora (North-Holland, Amsterdam, 1987), pp. 629–711.

[18]W. van Saarloos, Phys. Rev. A **37**, 211 (1988).

[19]J. S. Langer (private communication); W. van Saarloos (private communication).

[20]H. Guo and D. Jasnow, Phys. Rev. A **34**, 5027 (1986); D. Jasnow, Supperlattices Microstructures, **3**, (6), 581 (1987).

[21]S. Sarkar (private communication).

[22]H. Chou and H. Z. Cummins, Phys. Rev. Lett. **61**, 173 (1988).

[23]A. Dougherty, P. D. Kaplan, and J. P. Gollub, Phys. Rev. Lett. **58**, 1652 (1987).